

GT2011-468*)

COMPUTATIONAL STUDY ON THE EFFECT OF LOCAL EXPANSION AND CONTRACTION UPON SURFACE DEPOSITION IN A HEATED FUEL INJECTOR

Ehsan Alborzi
Mechanical Engineering,
University of Sheffield,
S1 3JD, Sheffield, UK

Renato Piazzolla
Mechanical Engineering,
University of Sheffield,
S1 3JD, Sheffield, UK

Christopher Wilson
Mechanical Engineering,
University of Sheffield,
S1 3JD, Sheffield, UK

ABSTRACT

A preliminary numerical analysis was carried out to examine the effect of local expansion and contraction on surface deposition rate for two series of geometries. These geometries correspond to the new geometrical features found in jet fuel injection system. For this simulation, commercial computational fluid dynamic package, Fluent 6.3.26, was used. Fluid flow, energy, and turbulence equations were solved coupled with a pseudo-detailed chemical kinetic model for jet fuel thermal degradation and the subsequent surface deposition sub model. The model results indicate that the highest deposition rates occur at intermediate expansion ratios and for a bigger inlet diameter due to a lower convective heat transfer. It was also shown that high expansion ratios are recommended to be used for short injector lengths. These simulated results are used for the experimental work in progress. The most susceptible locations to surface deposition are those with the highest rates; these are the best indicative points for data sampling.

INTRODUCTION

In modern aircraft, jet fuel serves a dual purpose as both fuel and as the primary heat sink to dissipate waste heat from aircraft subsystems and engines [1]. Due to cooling heat transfer loads, jet fuel's temperature increases thus promoting fuel thermal degradation. Thermal degradation is manifested

by formation of soluble and insoluble materials in bulk fuel. These materials contribute to the deposition of carbonaceous particles on the fuel wetted surfaces in the fuel system [2]. The engine performance and its durability are severely affected by the growth deposit in different parts of the fuel system. Clogging and blockage of fuel nozzles, injectors, obstruction of close-tolerance valves and actuators are some examples of the detrimental effects of jet fuel thermal degradation [3]. The most pertinent consequence of jet fuel thermal degradation is that of deposit growth upon surfaces used for cooling heat exchange within the engine. In extreme cases the growth of insulating carbonaceous deposits result in a temperature increase on the external tube wall, nullifying or inverting the fuels efficacy as a cooling agent. Thermal stability is defined as the tendency of a liquid jet fuel to form solid deposits via a multitude of physico-chemical interactions [4]. These depend on a number of factors including chemical composition of jet fuel, temperature, duration of thermal exposure, flow pattern; physico-chemical characteristics of fuel wetted surface amongst others [4] [5].

Due to the significance of fuel thermal stability as a limiting factor in fuel system design, it is very desirable to create appropriate models capable of predicting various features of thermal stability for a wide range of conditions and geometries similar to those encountered in real jet fuel system. Advances in capacity of digital computers to store data and to perform

algebraic equations have significantly facilitated the solution of numerical models. This resulted in the progress of CFD models allowing for a broad range of applications in different engineering problems. However, the consistency of the numerical model is restricted to a number of parameters such as the robustness of physical model and the computational techniques applied for the solution of mathematical models. Solution of these equations can be rather complicated for most engineering applications due to the complexities caused by geometries, flow pattern, three dimensionality, the precision of boundary conditions, convergence criteria, and the interpretation of the numerical solution. Even with a simple geometry such as a cylindrical flow passage, numerical simulation will be approximated and hence accompanied by errors. As a result of the complex flow chemistry and flow physics mentioned the computational effort required to model the entire aircraft fuel system effectively is currently deemed impractical.

Determination of a physical model of jet fuel thermal stability has been a research topic for both fuel producers and jet engine manufacturers. Many aspects of this problem have been ascertained over recent decades; however there are still numerous uncertainties. This can be attributed to the fact that every single intermediate species must be accounted for in a comprehensive model causing great computational multiplicity/complexity. In addition, chemical composition of jet fuel varies from one fuel sample to the next. A simpler approach is to construct the model based on the study of a prototypical fuel component under controlled conditions of known temperature in an experimental regime that minimises the impact of physical processes related to the fluid flow. Subsequently, this method can be extended to binary, ternary, and quaternary mixtures.

Choosing n-dodecane as the surrogate fuel, Boss and Hazlett [6] reported that at moderate temperatures the processes leading to surface deposition are initiated from a chain reaction mechanism known as autoxidation. Autoxidation is initiated by the reaction of fuel components with dissolved oxygen, its rate being dependent on temperature within the range of approximately 260 to 480 °C. Various soluble and insoluble species are generated during the autoxidative reactions. The insoluble materials contribute to a collection of ambiguous particle-surface interactions which form the carbonaceous deposit layer.

CFD techniques incorporating realistic chemistry mechanism for thermal stability offer the potential of being applied as research tools to study surface deposition, particularly for the vulnerable parts of jet fuel system. Krazinski et al [7] incorporated a three step global chemistry model of jet fuel thermal decomposition into a computational fluid dynamic code that solves the Reynolds-averaged conservation equations of mass, momentum, and energy. The chemistry model was

assumed to be initiated with a two step global scheme for the simulation of jet fuel autoxidation and surface deposition processes. These processes were modelled assuming that all precursor species transported and adhered to the wall creating a deposit. The kinetic parameters for the surface deposition were calibrated in a way to reproduce a particular experimental condition.

Reddy and Roquemore [8] developed a time dependent CFD model with a global chemistry scheme simulating deposit build up and its impact on the fuel flow field together with heat transfer rate and their total impact on the rate of surface deposition. The time dependent Navier-Stokes equations along with the species continuity and energy equations are solved in an uncoupled manner using a fully implicit scheme. Reddy and Roquemore used the global chemistry model suggested by Krazinski et al, but also assumed that surface deposition rate increases as a power of deposit thickness. Katta and Roquemore [9] developed a time dependent CFD model to simulate the reciprocal impact of fluid flow and heat transfer on surface deposition for a jet engine injector feed arm. Turbulent-flow simulations for the flow bounded by the fuel deposit interface were made on a body-oriented coordinate system. The fuel thermal degradation mechanism was treated using a four step global reaction chemistry model similar to the Krazinski model. An extra reaction was added to simulate the surface deposition induction period associated with the slower deposition during the initial hours of thermal exposure. In this case the rate of the reaction occurring at the wall is expressed as a function deposit thickness. A more comprehensive global chemical kinetic mechanism of jet fuel autoxidation was used for the application in computational fluid dynamic by Katta et al [10]. It was assumed that the bulk fuel reaction kinetic with dissolved oxygen changes from zero order to the first order when dissolved oxygen concentration falls below 10 ppm. This model successfully simulates behaviour in some controlled cases, however still fails to predict the complex behaviour of fuel thermal degradation and product deposition when naturally occurring antioxidants are present in the fuel.

Advancements in the chemistry of jet fuel thermal degradation resulted in the construction of a pseudo-detailed mechanism tailored for liquid phase jet fuel autoxidation, see Zabarnick and Kuprowicz et al [11]. It was shown by Zabarnick et al [4] that different thermal oxidative propensities among a series of jet fuel samples are due to different concentrations of the heteroatomic species present in such jet fuel samples. The concentration of these species is of the order of parts per million. These species include oxygen-containing molecules (hydroperoxides, phenols), sulphur containing molecules (thiols, sulfides, disulfides, Benzothiophenes, and elemental sulphurs), and nitrogen containing molecules (anilines, pyridines, indoles, amines and carbazoles). Pseudo-detailed mechanism focuses on the contribution of such classes of

species in more sensitive reactions. Pseudo-detailed mechanism has been used in conjunction with the CFD for simulation of dissolved oxygen consumption as well as surface deposition in geometries and conditions similar to the apparatus, in which the mechanism was validated, see Ervin et al [12], Kuprowicz et al [11]. We applied a transient, two dimensional axis symmetric CFD calculation using the pseudo-detailed mechanism suggested by Zabarnick for the autoxidation and a cumulative surface deposition chemistry based on moving boundary technique. In order to include the sticking probability in transient/moving boundary CFD calculation as suggested by Ervin et al, a user defined function was developed by Alborzi [13] that was validated against the experimental data taken from the Aviation Fuel Thermal Stability Test Unit(AFTSTU), see Blakey and Wilson [14].

We performed a series of preliminary and simplistic CFD calculations to examine the effect of local contraction/expansion upon surface deposition for two series of geometries corresponding to the new geometrical features that can be found in a jet fuel injection system. The results of modelling are used for the experimental part of the work in progress to identify the locations of thermocouples for which are more susceptible to the surface deposition. Transient CFD calculations will be required in future for these geometrical features to investigate the mutual effect of blockage on heat transfer characteristics, fluid flow, and surface deposition rate.

Computational Fluid Dynamic

To simulate the effect of expansion diameter on tendency to surface deposition, the species, temperature, and velocity distributions were obtained by the finite volume solution of the species, enthalpy, Navier-Stokes, and turbulent energy equations. Descriptions of these equations can be found in various computational fluid dynamic text books. The source term for precursor species is provided from the solution of ordinary differential equations representing the pseudo-detailed mechanism of jet fuel thermal stability. No turbulence-chemistry interaction was included for the modeling; hence, the chemistry scheme was solved by using the laminar finite rate model. Mass diffusion equations were then used to calculate the transport of precursor species to the surface. As for surface deposition, wall reaction was employed. Two series of geometries corresponding to the contraction/expansion nozzles were created for the CFD analysis. As fig 1 indicates the total length of the tube is 310 mm. The tube outer diameter is 6 mm while the inner diameter (labeled as d) varies amongst the created geometries. The inner diameter expands to the larger diameter (labeled as D). At a distance of 290mm tube inlet downstream, the expanded tube contracts to the smaller diameter (d). 10 mm of smaller tube from each side and the entire expanded region are subject to the thermal exposure. The first series include the geometries with the contraction diameter of 2 mm and varying expansion diameter from 2-5

mm while the second series has the contracted diameter of 1 mm and varying expansion diameter from 2-5 mm. For instance, case d2D4 indicates the geometry which has 2 mm contraction diameter at the inlet and 4 mm diameter at the expansion stretch. Only half sections of the geometries were created in Gambit in a way to be compatible with the two dimensional axis symmetric solutions in Fluent. Two continuum types were specified for all geometries, one allocated to the fluid region for the solution of fluid flow, energy and species and the other specified as solid for the calculation of heat transfer from the stainless steel towards the jet fuel. Quadrilateral structured mesh was chosen for the geometries with the higher density at the proximity of each expansion-contraction-expansion. In all cases the same fuel mass flow rate (15 kg/h), net constant heat flux (25000 W/m²) and fuel inlet temperature (185 °C) were used. No heat lost from the walls term was included in this modeling. Jet fuel was assumed to be an incompressible fluid and an inlet velocity of 2 m/s corresponding to the mass flow rate and jet fuel inlet temperature was used for all cases. The choice of jet fuel chemical composition was arbitrary and identical to a slow oxidizing fuel sample (F3219) from the work published by Kuprowicz et al. Therefore in conformity with the pseudo detailed mechanism the molar concentration of the fake initiator species was set to 1e-8 M and the concentration of oxygen was set to 1.5 mM, the value corresponding to the 70 ppm dissolved oxygen in jet fuels. As the chemical composition of jet fuel from the fuel tank up to the feed arm interjector is subject to compositional change, a perfectly stirred reactor calculation was performed to estimate the change of fuel chemical composition with respect to the different thermal regimes and residence time that can be encountered in a real jet fuel system. The operational parameters for the reactor calculations were in line with the values of the high pressure system in the Aviation Fuel Thermal Stability Test Unit [14]. Three user defined functions were created to address the change of density, and the viscosity of jet fuels. Variation of these properties with temperature is given in appendix.

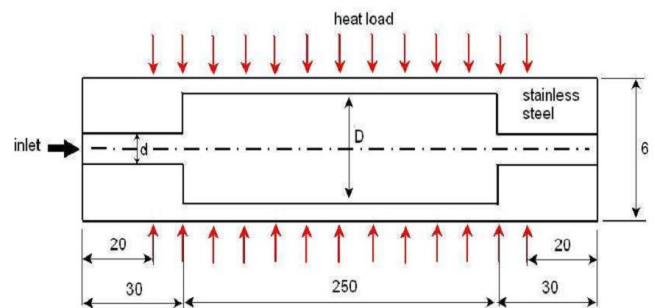


Figure 1: the outline of the computational domain (in mm)

Results and Discussion

The first CFD calculation was performed to model a simple straight tube d2D2. As indicated in fig 2 bulk fuel varies linearly along the tube while the temperature profile at the fuel wetted surface exhibits a 15 °C in the first 20 mm of the tube. This change in temperature is due to conductive heat transfer through the stainless steel. From this point, corresponding to the beginning of the thermal exposure region temperature increases linearly reaching a maximum of around 215 °C at an axial distance of 280mm where the thermal stress region ends. Non contact, thermal fuel stressing experimental apparatus can be modeled using such a simulation. From this point onward the tube is not subject to direct thermal exposure and the temperature decreases for the next 30 mm from 215 °C to 200°C due to the cooling effect of moving jet fuel. It was shown by Kuprowicz et al that a slow oxidizing jet fuel such as F3219 consumes all oxygen within approximately 6 minutes. However, because of the low residence time that an element of flow spends inside the tube like d2D2, the autoxidation reaction is far from completed. It is shown in fig 2 that only a small fraction of the total amount of dissolved oxygen is consumed in the tube. These modeling scenarios showed that the temperature of bulk fuel is independent of the change of pipe diameter for expansion/contraction. This result occurs because the total fuel mass flow rate and heat flux are constant amongst all geometries. Since the value of heat capacity is the same for the jet fuel in all geometries, the temperature gradient between the tube inlet and outlet is the same. The temperature profiles along with the deposition rates for three sections (prior to the heated zone, heated zone and after heated zone) are presented in fig 3 and fig 4. The results indicate that for the first 20 mm along the tube all tubes exhibit the same amount of deposition, however, there is a propensity for the results to vary within the expanded passage amongst all geometries. It can be seen that within the expansion passage, surface deposition increases for d2D2 to d2D3 with the highest tendency of deposition related to d2D4. This is more clearly depicted in fig 5 in which the maximum deposition rate is plotted for different expansion diameters. This indicates that the maximum deposition rate increases from d2D3, as the diameters increase, reaching a maximum for the geometry corresponding to d2D4 after which it decreases for d2D5. Such decrease from d2D4 to d2D5 is related to the change of the flow pattern due to the vorticity (see fig 6 and fig 7) and hence the change of residence time caused by the effect of the expansion. The impact of expansion upon heat transfer rate and turbulence is pronounced up to an axial distance of 80 mm from the tube inlet (50 mm after the expansion diameter) after which it begins to fade away.

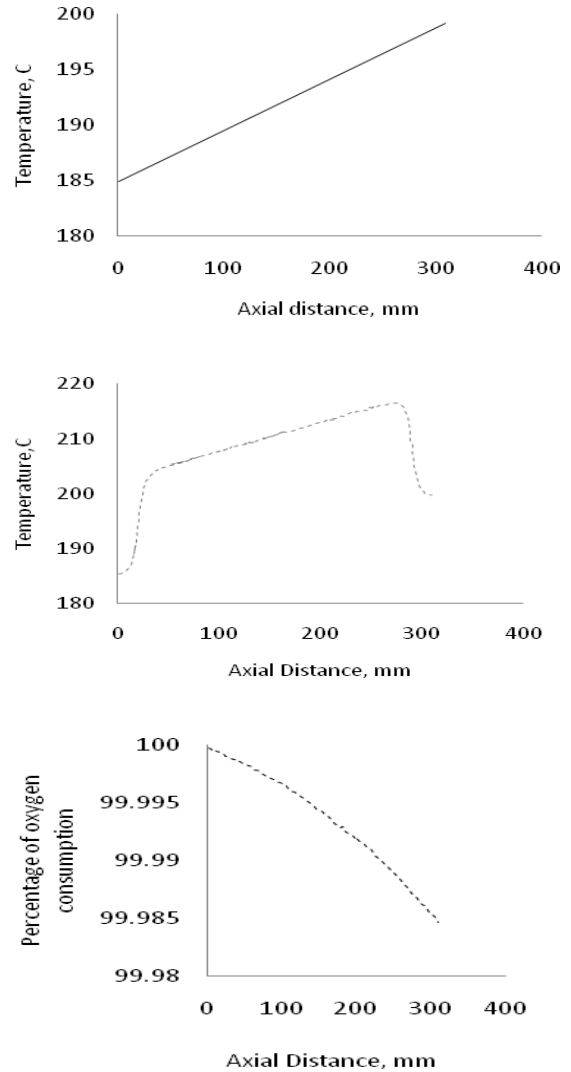


Figure 2: modelling results of bulk fuel temperature, wall temperature, surface deposition, and oxygen consumption for d2D2 geometry

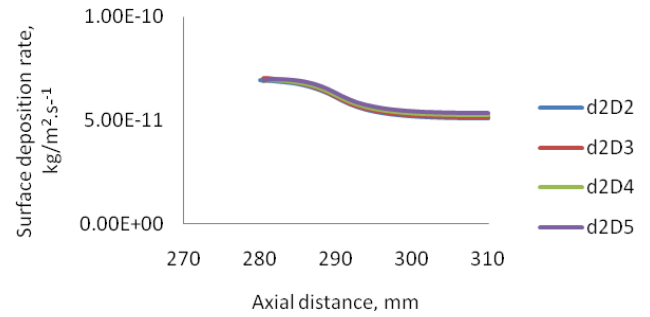
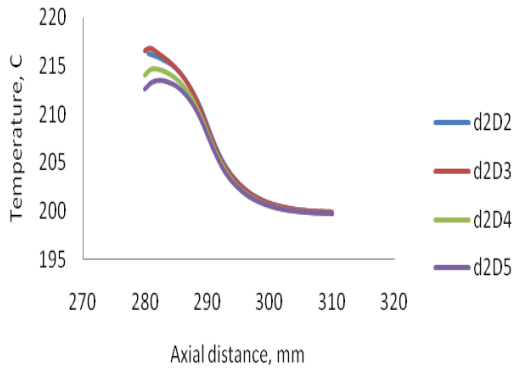
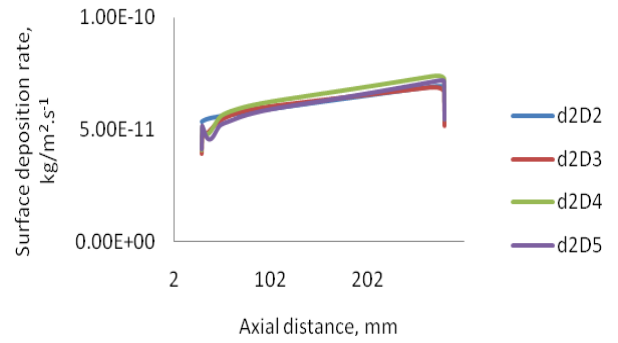
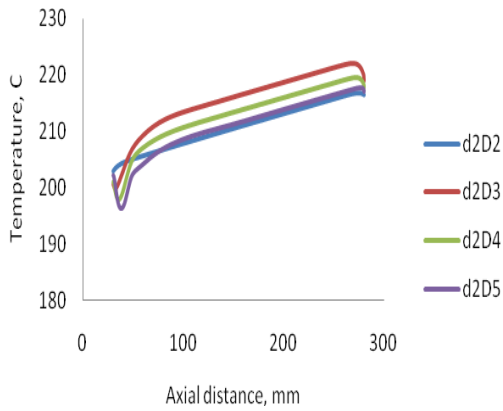
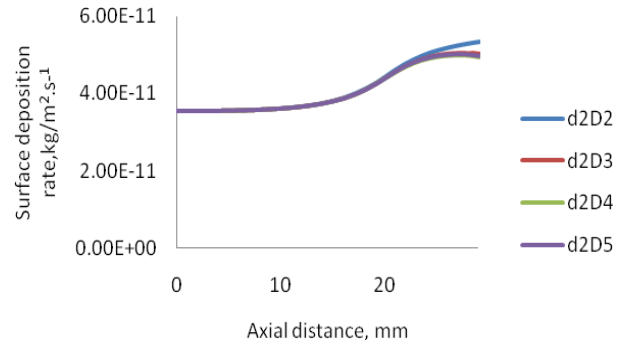
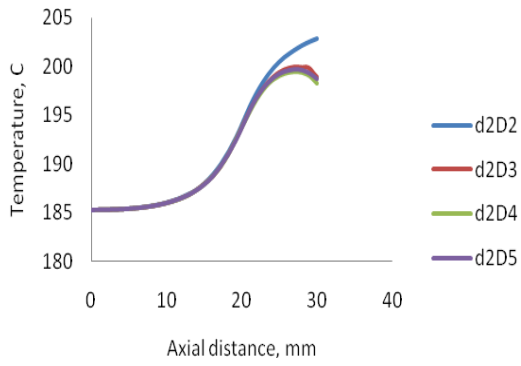


Figure 3: wall temperature profile for three sections (prior to the heated zone, heated zone and after heated zone) for d2Dx geometries

Figure 4: surface deposition rate for three fuel wetted walls (prior to the heated zone, heated zone and after heated zone) for d2Dx geometries

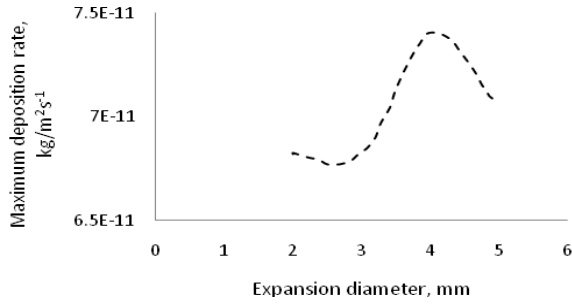


Figure 5: profile of maximum surface deposition rate for different expansion diameter of first series of geometries (d2Dx)

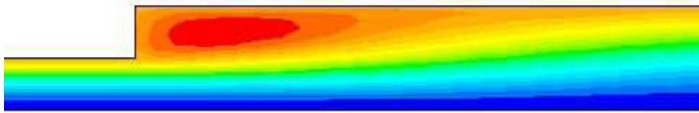


Figure 6: contour of stream function

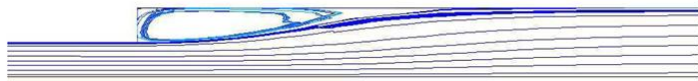


Figure 7: path line of some particles coloured by residence time

It can be seen from fig 3 that the maximum wall temperature is achieved by d2D3 in spite of the fact that it exhibits a lower deposition propensity in comparison to d2D4 and d2D5 respectively. This can be rationalized using the convective heat transfer equation:

$$Q = h_c \cdot A \cdot \Delta T$$

Where h_c denotes the convective heat transfer coefficient, A represents the surface area of heat transfer, ΔT is the temperature drop between wall and bulk fuel and Q is the rate of heat transfer. Since Q is constant ΔT is proportional to the inverse of product of A and h_c . The surface area is directly proportional to the diameter whereas the convective heat transfer coefficient is a function of Nusslet number which in turn depends upon both Reynolds number and Prandtl number. Therefore, we plotted both A and h_c with respect to the values corresponding to the expansion diameters as presented in fig 8. The convective heat transfer coefficient decreases with the expansion diameter due to the reduced velocity while the area increase. This indicates that the product of h_c and A reaches to a minimum for the point which corresponds to the 3 mm

expansion diameter while the temperature diameter is the maximum at this point. The latter is plotted in fig 9.

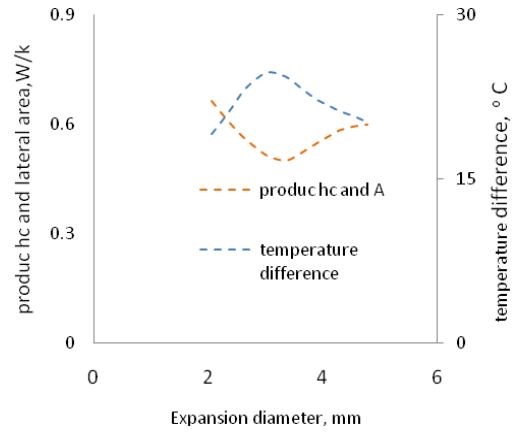


Figure 8: calculations of convective heat transfer parameters for d2Dx

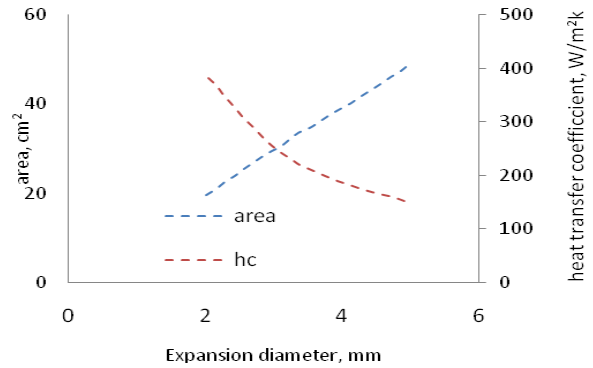


Figure 9: plot of heat transfer coefficient and area with respect to the expansion diameter

The surface deposition in the second series of geometries is similar to the first series as indicated in fig 11, although all geometries exhibit a higher rate in comparison to the d2Dx series of geometries. The maximum deposition rate is achieved by d1D3 case, whereas the maximum deposition for the first series occurs in d2D4. Similar to the first series of geometries, the maximum point for d1D3 corresponds to an axial distance of 80 mm, the point at which the impact of vorticity caused by the expansion is the strongest. It can be seen from surface deposition graphs for both series of geometries that the gradient of deposition rate differs in each case, even with the linear region. The larger diameter cases exhibit the greatest gradient, suggesting that for an infinite pipe length, this would provide the greatest surface deposition. With respect to the wall temperature, the profile is similar to the first series of

geometries, although, all the second series geometries exhibit lower values with the maximum wall temperatures attained by d2D3 as presented in fig 10. Similar convective heat transfer analysis explains the reason of highest value of wall temperature for this geometry.

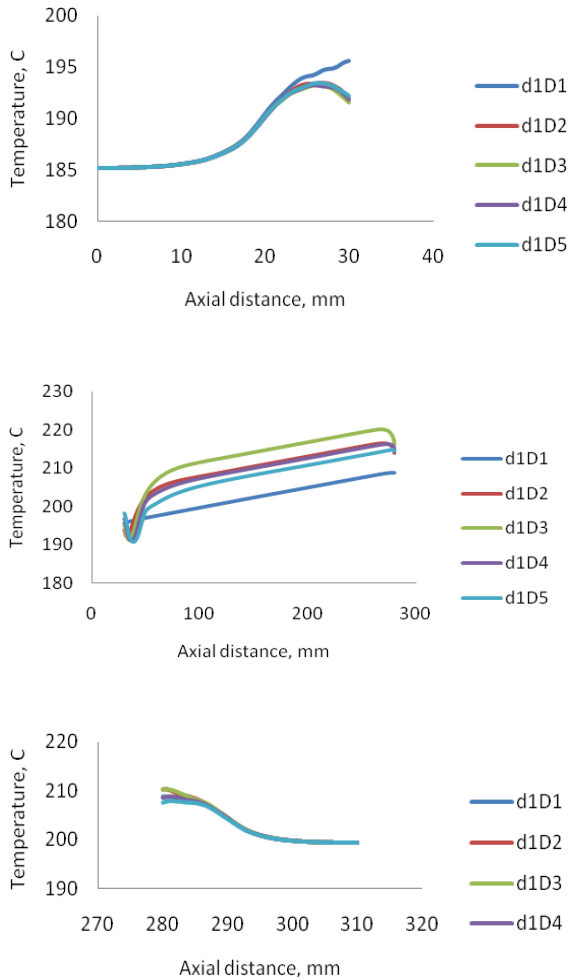


Figure 10: wall temperature profile for three sections (prior to the heated zone, heated zone and after heated zone) for the d1Dx geometries

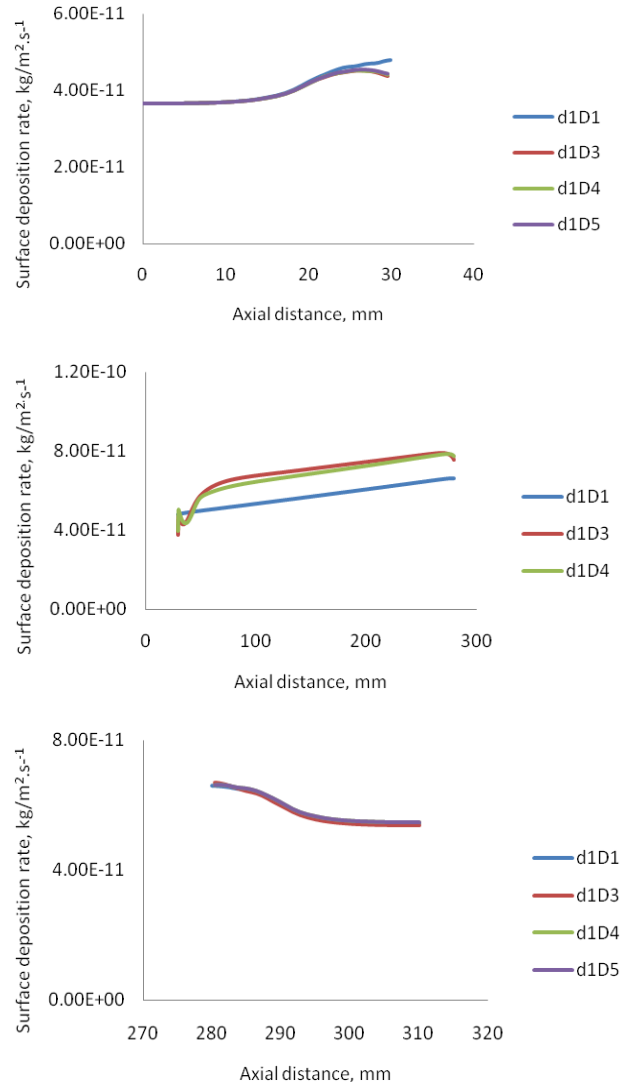


Figure 11: surface deposition rate for three fuel wetted walls (prior to the heated zone, heated zone and after heated zone) for d1Dx geometries

Conclusion

Deposit thickness is directly linked to the surface deposition rate; however, the accurate calculation of deposit growth in some vulnerable parts of jet fuel system necessitates the development of time dependent physical model. Once this is available, it can be incorporated to the time dependent Navier-Stokes equations. By the application of moving boundaries surface deposition can be modeled in a transient calculation. Since the physical model is not yet available for such geometrical features, we performed steady state calculations using a pseudo-detailed mechanism for jet fuel autoxidation along with a subsequent wall reaction sub model. The results

of these simulations are used for identifying the best locations of data (temperature) recording for an in process work. In addition, the modeling results can be used to rank the contraction-expansion tubes which are similar to the new geometrical features encountered in jet engine injection systems. It was shown that at regular expansion ratios, the rate of surface deposition immediately after the expansion was the highest, hence are not advised in practice for short injectors. The application of higher expansion ratios lead to lower surface deposition with respect to the diameter enlargement, however, at the same time they have the highest deposition rate gradients which results in higher deposition rate for a longer fuel injector. Tubes with higher inlet expansion diameter results in higher deposition propensities.

References

1. Hazlett, R.N. *Thermal Oxidation Stability of Aviation Turbine Fuels*. 1991, American Society for Testing and Materials (ASTM).
2. Jones, E.G and Balster, W.J. *Phenomenological Study of the Formation of Insolubles in Jet-A Fuel*. Energy and Fuels, 1999, vol 7, p. 968-977.
3. Dagget, D.L, Veninger, A, Lewis, C, Bullock, S and Kamin, R. *The Development of an Aviation Fuel Thermal Stability Test Unit*. Journal of Engineering for Gas Turbines and Power, 1995, vol 117, p. 468-473.
4. Zabarnick, S. *Chemical Kinetic Modeling of Jet Fuel Autoxidation Chemistry*. Ind.Eng.Chem.Res, 1993, vol 32, p.1012-1017.
5. Jones, E.G, Blaster, L.G and Blaster, W.J. *Autoxidation of Aviation Fuels in heated tubes: Surface effect*. Energy and Fuels, 1996, vol 10: p. 831-836.
6. Boss, B.D. and Hazlett, R.N. *n-Dodecane Oxidation-Elucidation by Internal Reference Techniques*. Ind. Eng. Chem.Prod.Res.Dev, 1975, vol 14, p. 135-138.
7. Krazinski, J.L., S.P. Vanka, J.A. Pearce, and Roquemore, W.M. *A Computational Fluid Dynamics and Chemistry Model for Jet Fuel Thermal Stability*, 1990, ASME.
8. Reddy, K.T, Roquemore, W.M. *A Time-Dependent Model with Global Chemistry for Decomposition and Decomposition and Deposition of Aircraft Fuels*, Symposium on the Stability and Oxidation Chemistry on Middle Distillate Fuels, 1990, Washington Meeting, August 26-31.
9. Katta, V.R. and Roquemore, W.M. *Numerical Method for Simulating Fluid-Dynamic and Heat Transfer Changes in Jet-Engine Injector Feed Arm Due to Fouling*, Journal of Them physics and Heat Transfer, 1993, vol 7, p. 651-660.
10. Katta, V.R, Jones, E.G and Roquemore, W.M. *Modeling of Deposition Process in Liquid Fuels*. Combustion Science Technology, 1998, vol 139, p. 75-111.
11. Kuprowicz, N.J, Zabarnick, S, West, Z.J and Ervin, J.S. *Use of Measured Species Class Concentrations With Chemical Kinetic Modeling for the Prediction of Autoxidation and Deposition of Jet Fuels*, Energy and Fuels, 2007, vol 21, p. 530-544.
12. Ervin, J.S, Zabarnick, S and Williams, T.F. *One Dimensional Simulations of Jet Fuel Thermal Oxidative Degradation and Deposit Formation within Cylindrical passages*. Journal of Energy Res.Tech, 2000, vol 122, p. 229-238.
13. Alborzi, E. *An Investigation into Carbon Deposition Growth in Jet Engine Injector Feed Arm due to Fuel Thermal Degradation*, in Mechanical Engineering, 2009, University of Sheffield
14. Blakey, S.G and Wilson, C.W. *AFTSTU test report: Baseline tests, 2008*, The University of Sheffield, Department of Mechanical Engineering.
15. Moses, C.A. *Development of the Protocol for Acceptance of Synthetic Fuels under Commercial Specification, 2007*, Fuels and Lubricants Technology Department Southwest Research Institute (SWRI), San Antonio, Texas.

APENDIX A

Species	Molecular Weight	Mass Fraction	Diffusion Coefficient
Initiator	169	1.99E-9	1E-8
R	169	7.25E-13	1E-8
O ₂	32	7.19E-5	1E-8
RO ₂	201	1.05E-12	1E-8
RH	170	bulk species	1E-8
RO ₂ H	202	1.35E-6	1E-8
Termination1	402	1.17E-12	1E-8
Termination2	370	1.07E-12	1E-8
R ₂	338	1.52E-13	1E-8
RO	185	1.14E-19	1E-8
OH	17	2.21E-17	1E-8
ROH	186	7.98E-13	1E-8
Rprime	169	2.20E-16	1E-8
Carbonyl	16	1.45E-10	1E-8
H ₂ O	18	1.64E-10	1E-8
ROterm	370	1.71E-26	1E-8
A	200	2.18E-9	1E-8
ProductsAH	402	1.61E-9	1E-8
SH	200	6.25E-4	1E-8
ProductSH	402	9.15E-7	1E-8
Alkane	170	1.55E-9	1E-8
AH	201	2.51E-5	1E-8
Metal	64	4.00E-10	1E-8
Soluble	402	1.58E-9	1E-8
Insoluble	402	3.15E-11	1E-10

Table1: Species boundary condition for AFTSTU nozzle inlet with relevant molecular weight

T [K]	Density [kg/m ³]	Dynamic [kg/ms]
273.14	820.559	2.20E-003
283.14	813.033	1.78E-003
293.14	805.486	1.47E-003
303.14	797.917	1.22E-003
313.14	790.325	1.04E-003
323.14	782.706	9.19E-004
333.14	775.06	8.20E-004
343.14	767.384	7.35E-004
353.14	759.676	6.64E-004
363.14	751.934	6.02E-004
373.14	744.154	5.49E-004
383.14	736.333	5.03E-004
393.14	728.468	4.62E-004
403.14	720.555	4.27E-004
413.14	712.588	3.95E-004
423.14	704.564	3.67E-004
433.14	696.475	3.42E-004

Table 2: Variation of density and viscosity of jet fuel with temperature[15]